LiNi$_{1/3}$Co$_{1/3}$Mn$_{1/3}$O$_2$ Nanoplates with {010} Active Planes Exposing Prepared in Polyol Medium as a High-Performance Cathode for Li-Ion Battery

Jili Li, Ruimin Yao, and Chuanbao Cao*

Research Centre of Materials Science, Beijing Institute of Technology, Beijing 100081, China

S Supporting Information

ABSTRACT: As we know, Li$^+$-ion transport in layered Li-Ni$_{1/3}$Co$_{1/3}$Mn$_{1/3}$O$_2$ (NCM) is through two-dimensional channels parallel to the Li$^+$-ion layers that are indexed as {010} active planes. In this paper, NCM nanoplates with exposed {010} active facets are synthesized in a polyol medium (ethylene glycol) and characterized by XRD, XPS, SEM, and HR-TEM. In addition, the effects of reaction conditions on the morphologies, structures and electrochemical performances are also evaluated. The results show that more {010} facets can be exposed with the thickness of NCM nanoplates increasing which can lead to more channels for Li$^+$-ion migration. However, when the annealing temperatures exceed 900 °C, many new crystal planes grow along the thickness direction covering the {010} facets. In all of the NCM nanoplates obtained at different conditions, the NCM nanoplates calcined at 850 °C for 12 h (NCM-850-12H) display a high initial discharge capacity of 207.6 mAh g^{-1} at 0.1 C (1 C = 200 mA g^{-1}) between 2.5 and 4.5 V higher than most of NCM materials as cathodes for lithium ion batteries. The discharge capacities of NCM-850-12H are 169.8, 160.5, and 149.3 mAh g^{-1} at 2, 5, and 7 C, respectively, illustrating the excellent rate capability. The superior electrochemical performance of NCM-850-12H cathode can be attributed to more {010} active planes exposure.

KEYWORDS: {010} active facets, nanoplates, polyol medium, LiNi$_{1/3}$Co$_{1/3}$Mn$_{1/3}$O$_2$, lithium-ion battery, cathode
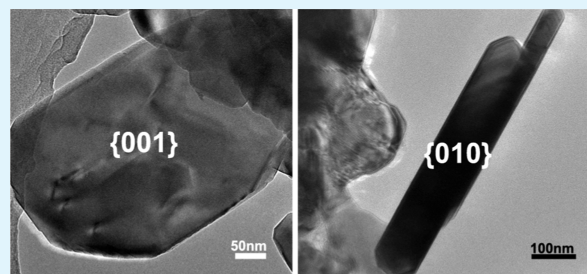
INTRODUCTION

Rechargeable lithium-ion batteries (LIBs), the dominant power source for portable electronic products, have also gained enormous interest for high power and energy density applications, such as electric vehicles (EVs), hybrid electric vehicles (HEVs) and stationary energy storage.[1−4] To meet the large-scale requirements of these applications, many researchers are focusing on the cathode materials with high capacity and rate capability. LiNi$_{1/3}$Co$_{1/3}$Mn$_{1/3}$O$_2$ (NCM), as one of the promising cathodes, has been widely investigated because of its high reversible capacity, relatively low cost, stable structure, and thermal stability.[5−13] Substantial research has indicated that conventional micrometer-sized bulk materials reach their intrinsic limits in electrochemical performance and unable to meet the increasing requirements. Nanostructures have been recognized as an effective strategy to solve these problems and improve the electrochemical performances of NCM materials. Therefore, various nanostructures, such as nanoparticles,[7] nanowires,[8] nanobricks,[9] hollow spheres,[10,11] and porous materials,[12,13] have been fabricated. This research illustrates that the performances of electrode materials depend strongly on the structure of nanomaterials. Thus, structurally and morphologically controlled synthesis of NCM nanostructures still remains a great challenge.

NCM with a hexagonal layer α-NaFeO$_2$ structure has a two-dimensional tunnel for Li$^+$-ions diffusion along the a (or b) axis.

The tunnel is parallel to the Li$^+$-ions layers including (010), (0$\overline{1}$0), (100), (110), (1$\overline{1}$0) and ($\overline{1}$00) planes denoted as {010} facets.[9] The layers perpendicular to the c-axis are indexed as {001} planes, which are composed of the corner-sharing NiO$_6$, CoO$_6$, and MnO$_6$ octahedra. Since the {001} planes cannot provide an appropriate path for Li$^+$-ions transportation, they are not electrochemically active. Therefore, NCM nanostructures with exposing {010} active facets can significantly improve the electrochemical performance. However, the {010} planes of NCM have higher surface energy than {001} planes through calculation.[9,14] As high-energy planes grow faster than low-energy ones, the high-energy planes tend to disappear during growth leading to the resulting crystal dominated by low-energy planes. It is illustrated that NCM with the {001} inert planes are thermodynamically stable products. Therefore, it is very difficult to prepare NCM with the {010} active facets exposure, in addition to its intrinsic lamellar structure. G.-Z. Wei reported hexagonal layer NCM nanobricks with the {010} active facets exposure by a solid-state reaction of LiOH·H$_2$O and nickel−cobalt-manganese hydroxide precursor.[9] The precursor was prepared through a PVP-assisted co-precipitation process under

nitrogen atmosphere, which is too complicated to undoubtedly increase the cost of LIBs.

Recently, polyol medium was introduced into preparing nano-sized cathode materials ($LiFePO_4$,[15,16] $LiMnPO_4$,[17] etc), in which polyalcohol (polyol) acts not only as a solvent but also as a chelating stabilizer. In addition, the nanoplates are easily obtained from the polyol medium. Here, we use a polyol medium (ethylene glycol) to control preparation of the NCM nanoplates with exposing {010} active facets. The NCM nanoplates with more {010} planes exposure display high initial discharge capacities of 207.6 and 178.1 mAh g^{-1} at 0.1 and 1 C (1 C = 200 mA g^{-1}) between 2.5 and 4.5 V as a cathode of LIBs, respectively. The NCM nanoplates also exhibit high rate capability.

EXPERIMENTAL SECTION

Preparation of NCM Nanoplates. Firstly, 10 mmol each of $Ni(NO_3)_2 \cdot 6H_2O$, $Co(NO_3)_2 \cdot 6H_2O$, and $Mn(CH_3COO)_2 \cdot 4H_2O$ and 31.5 mmol of $LiNO_3$ (Ni:Co:Mn:Li = 1/3:1/3:1/3:1.05 in the molar ratio) were added to 200 mL of ethylene glycol under stirring for 8 h at 85 °C. It was then dried at 120 °C overnight to obtain a brown gel-like solid. After being carefully ground, the mixture was preheated at 450 °C for 5 h and calcined at 800−900 °C for 8−16 h in air to obtain the final products.

Characterization. The X-ray diffraction (XRD) patterns of all samples were collected on a PANalytical X-pert diffractometer (PANalytical, Netherlands) with Cu Kα radiation at 40 kV and 40 mA in the 2θ range from 10° to 80°. The elemental compositions were characterized using the energy dispersive spectroscopy (EDS) (Oxford INCA, Britain). The exact metal ion molar ratios of Li:Ni:Co:Mn in all the $LiNi_{1/3}Co_{1/3}Mn_{1/3}O_2$ nanoplates were calculated from the results of inductive coupled plasma atomic emission spectrometry (ICP-AES, ICAP-6300). Hitachi field-emission scanning electron microscopy (FE-SEM S-4800) was used to analyze the size and morphology of the samples. The structure was observed by transmission electron microscopy (TEM) through Tecnai G^2 F20. The oxidation states of Ni, Co and Mn were evaluated by X-ray photoelectron spectroscopy (XPS) (PHI Quanteral II, Japan) and the energy scale was adjusted based on the graphite peak at 284.5 eV in the C1s spectrum. The data were fitted using XPSPEAK41 program.

Electrochemical Tests. CR2025 coin cells were used to measure the electrochemical performances of all samples. A slurry of 80 wt % the samples, 10 wt % carbon black, and 10 wt % poly(vinylidene fluoride) (PVDF) binder in N-methyl-2-pyrrolidone (NMP) was casted on aluminum foil. And then dry it in vacuum at 120 °C for 12 h to prepare the cathodes. The cells were assembled in an argon-filled glove box (with O_2 < 1 ppm and H_2O < 1 ppm) using Li metal as the counter and reference electrodes. The separators were Celgard 2400 films and the electrolyte was a solution of 1 M $LiPF_6$ dissolved in ethyl carbonate/dimethyl carbonate/diethyl carbonate (EC/DMC/DEC) (1:1:1 v/v). The galvanostatically charge−discharge tests were carried out at different C rates between 2.5 and 4.5 V on a LAND CT-2001A cell test instrument at around 25 °C. Cyclic voltammetry (CV) curves were collected on IM6e electrochemical workstation in the potential range of 2.5−4.5 V (vs. Li/Li$^+$) and at a scan rate of 0.1 mV s^{-1}. Electrochemical impedance spectroscopic (EIS) measurements were carried out at room temperature with an IM6e electrochemical station over the frequency range between 100 kHz and 0.1 Hz and applying an AC signal of 5 mV. The EIS data were fitted using the Zsimpwin 3.1 program.

RESULTS AND DISCUSSION

In the formation of $LiNi_{1/3}Co_{1/3}Mn_{1/3}O_2$ nanoplates with {010} active facets exposure, ethylene glycol plays a crucial role which acts not only as a solvent but also as a chelating reagent. The reactions of ethylene glycol with bi-functional groups and metal ions can generate a plate-like structure because of the

Table 1. The exact ratios of Li:Ni:Co:Mn from the ICP analysis

| | molar ratios of Li:Ni:Co:Mn | | | | |
	Li	Ni	Co	Mn	stoichiometries
NCM-800-12H	1.00	0.34	0.33	0.33	$LiNi_{0.34}Co_{0.33}Mn_{0.33}O_2$
NCM-850-12H	1.01	0.33	0.33	0.34	$Li_{1.01}Ni_{0.33}Co_{0.33}Mn_{0.34}O_2$
NCM-900-12H	0.98	0.33	0.33	0.34	$Li_{0.98}Ni_{0.33}Co_{0.33}Mn_{0.34}O_2$
NCM-850-8H	1.00	0.33	0.33	0.34	$LiNi_{0.33}Co_{0.33}Mn_{0.34}O_2$
NCM-850-16H	0.99	0.33	0.33	0.34	$Li_{0.99}Ni_{0.33}Co_{0.33}Mn_{0.34}O_2$
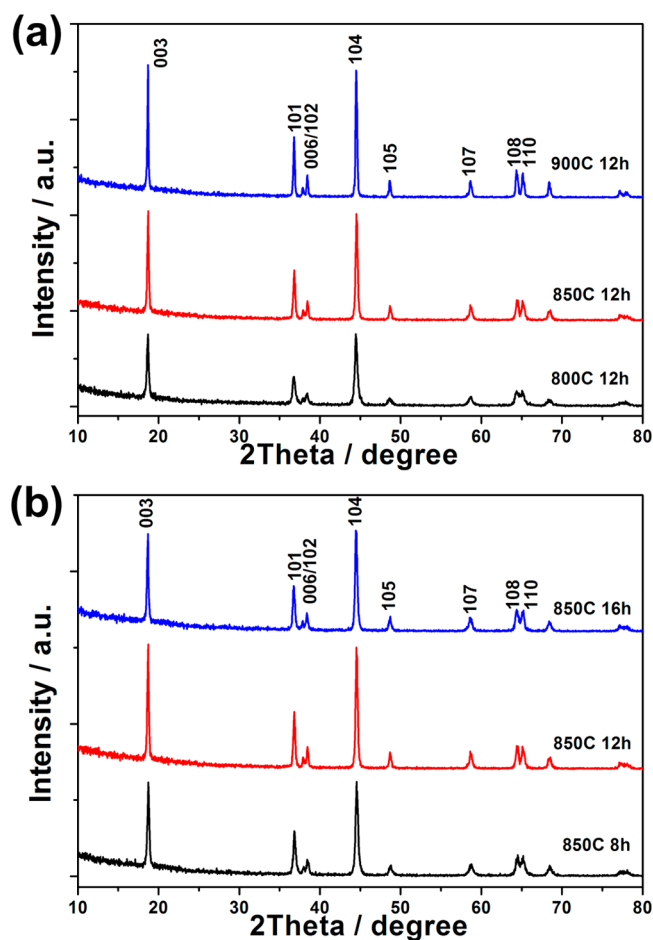
Figure 1. XRD patterns of the NCM nanoplates under different annealing conditions: (a) at different temperatures for 12 h, (b) at 850 °C for different sintering times.

hydrogen bond and chelating effects of ethylene glycol.[18] In addition, the larger viscosity of ethylene glycol slows the nucleation of the precursor.[9] In the formation process of platelike structure, the {001} facets are capped by ethylene glycol molecules at the same time, which enables slower growing rate along [001] leading to $LiNi_{1/3}Co_{1/3}Mn_{1/3}O_2$ nanoplates with {010} active facets exposure.

The atomic compositions of all the NCM nanoplates were measured by ICP-AES and the results of molar ratios are listed in Table 1. It is illustrated that the exact ratios of Li:Ni:Co:Mn in all the NCM nanoplates are approximately consistent with the expected $LiCo_{1/3}Mn_{1/3}Ni_{1/3}O_2$ stoichiometry within

5076

dx.doi.org/10.1021/am500215b | ACS Appl. Mater. Interfaces 2014, 6, 5075−5082
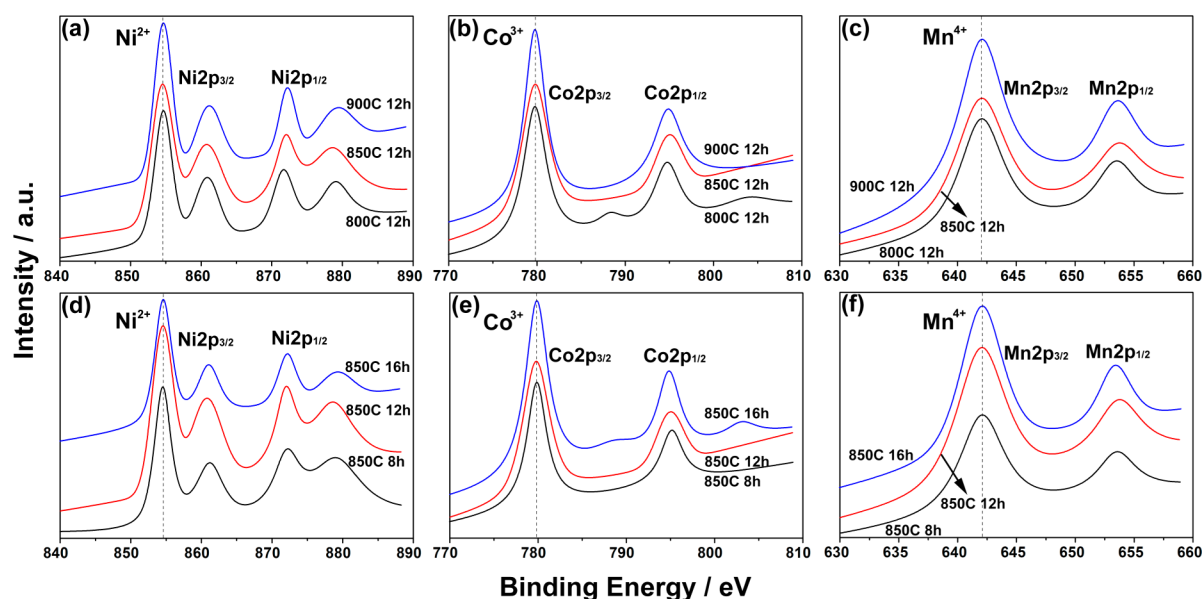
Figure 2. XPS spectra of Ni2p, Co2p, and Mn2p for all the samples. (a−c) The XPS spectra of (a) Ni2p, (b) Co2p, and (c) Mn2p for NCM nanoplates obtained at different temperatures for 12 h. (d−f) The XPS spectra of (d) Ni2p, (e) Co2p, and (f) Mn2p for NCM nanoplates sintering at 850 °C for different times.
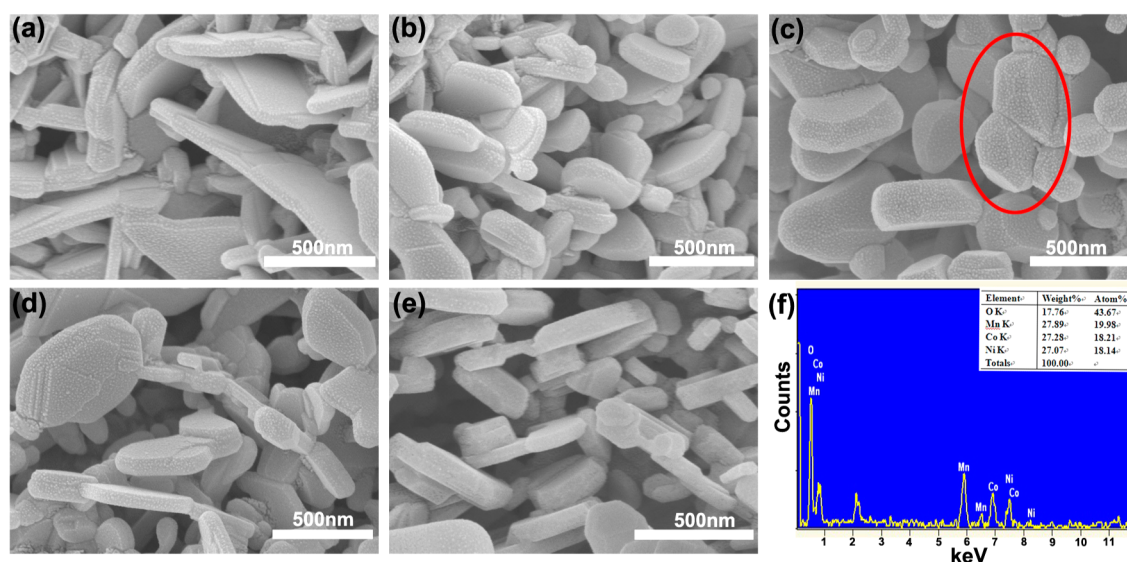
Figure 3. SEM images of NCM nanoplates obtained from different annealing conditions: (a) 800 °C, 12 h; (b) 850 °C, 12 h; (c) 900 °C, 12 h; (d) 850 °C, 8 h; (e) 850 °C, 16 h. (f) EDS results of the sample sintered at 850 °C for 12 h.

experimental errors. Compared with the starting molar ratio of Li:Ni:Co:Mn (1.05:1/3:1/3:1/3), minor Li source is lost during high-temperature procedure.[7]

The XRD patterns of all samples prepared with different annealing conditions are shown in Figure 1. All peaks can be indexed as a hexagonal α-NaFeO$_2$ structure (space group: R-3m) without any impurity phase in agreement with the pattern of a pure single phase of LiNi$_{1/3}$Co$_{1/3}$Mn$_{1/3}$O$_2$.[5,12] The clear separations of the (006)/(102) and (108)/(110) peaks for all of these samples suggest the formation of highly ordered hexagonal layered structure. The intensity ratio of (003) and (104) peaks $(I_{(003)}/I_{(104)})$ is always shown to be a measurement of the cation mixing.[12] When the value of $I_{(003)}/I_{(104)}$ is more than 1.2, it indicates a low cation mixing. However, in all of our XRD patterns, the values of $I_{(003)}/I_{(104)}$ are all smaller than 1.2 ascribing to the presence of Ni^{2+}-ions in the lithium layers. It

may also arise from the preferred orientation due to the special platelike structure.[19]

X-ray photoelectron spectroscopy (XPS) measurements (Figure 2) were carried out to gain more insight into the oxidation states of transition metals in the as-prepared NCM nanoplates. The peaks at binding energies of 854.5, 779.8, and 642.1 ($\pm$ 0.05) eV are attributed to Ni^{2+}, Co^{3+}, and Mn^{4+} in all the NCM nanoplates, respectively.[10,20] The observed XPS peak sites for all the NCM nanoplates are similar with each other, which indicates that the effects of annealing conditions on the oxidation states of Ni, Co, and Mn elements can be negligible.

The morphologies and microstructures of the as-prepared NCM nanoplates are shown in Figure 3a−e. From the SEM images of the samples, there are large amounts of disordered pores between the nanoplates because of the presence of ethylene glycol. The ethylene glycol can transform to volatile
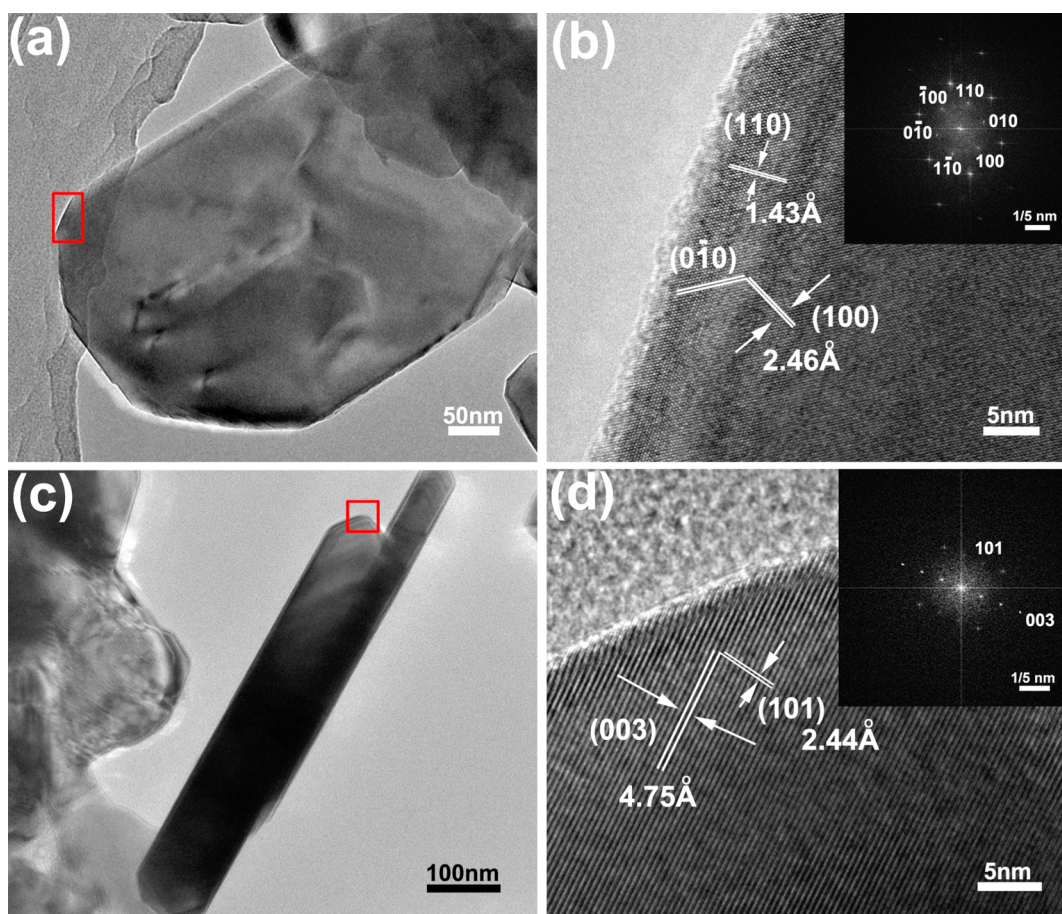
Figure 4. (a) TEM image of the frontal view of NCM nanoplates obtained at 850 °C for 12h (NCM-850-12H). (b) HRTEM image and Fast Fourier Transform (FFT) pattern of the frontal plane in a. (c) TEM image of the lateral view of NCM-850-12H. (d) HRTEM image and fast Fourier transform (FFT) pattern of the lateral plane in c.

products during the heating procedure leading to the porous structure. The porous structure can enable the facile electrolyte penetration.[13] The NCM nanoplates sintered at 800 °C for 12h (NCM-800-12H) (Figure 3a) clearly show 70−100 nm in thick and about 1 μm in width. In addition, the SEM image also reveals that the NCM nanoplates are composed of thinner domains (nanoplates) with thickness of about 10 nm. With the annealing temperature increasing (Figure 3a−c), the thickness of the $LiNi_{1/3}Co_{1/3}Mn_{1/3}O_2$ nanoplates is larger and the width is smaller attributing to the Ostwald Ripening mechanism with a template directed anisotropic growth process.[21] At the same time, some small NCM nanoplates form, which are not thermodynamic equilibrium and unstable. In addition, the growth rate along the surfaces of NCM nanoplates is slower than along the lateral planes because the surfaces of NCM nanoplates are capped by ethylene glycol molecules. Therefore, the thickness is larger and the width is smaller when the temperature increases. Continuing to raise the temperature, the small NCM nanoplates disappear and the thickness of NCM nanoplates continues to rise. However, because the high surface energy of lateral planes enables the thicker NCM nanoplates unstable, some new planes grow to reduce the surface energy along the thickness direction (elliptic zone in Figure 3c). It is noteworthy that the thinner domains disappear under sintering at 900 °C and the new crystal planes along the thickness direction may result from some of the layered structures trending to transform into a spinel structure.[9] The thickness

distribution and the average thickness of the NCM nanoplates at different sintering temperatures are shown in Figure S1 in the Supporting Information. On the other hand, when the sintering time is raised, the thickness of the NCM nanoplates (Figure 3b, d, and e) increases slightly. From the thickness distribution of the NCM nanoplates (see Figure S2 in the Supporting Information), the average thickness first increases and then decreases with the sintering time lengthening. It is caused by the thickness distribution of the sample calcined at 850 °C for 16h (NCM-850-16H) with two maximum at about 75 and 125 nm, respectively, leading to the lower average thickness. This phenomenon can be owing to the Ostwald Ripening.[21] The chemical composition of NCM nanoplates prepared at 850 °C for 12 h (NCM-850-12H) has been analyzed by EDS (Figure 3f). The results illustrate that the atomic ratio of the elements Ni, Co, and Mn is approximately 1:1:1 the same as the designed value and the results of ICP analysis.

The NCM nanoplates calcined at 850 °C for 12h (NCM-850-12H) are investigated by transmission electron microscopy (TEM) (Figure 4). From the frontal (Figure 4a) and lateral view (Figure 4c), the morphology and size of the nanoplates can be observed clearly in good agreement with the SEM results. Figure 4b shows the HR-TEM image of the frontal plane and its corresponding Fast Fourier Transform (FFT) pattern (the inset image). There are three sets of clear fringes. Two of them have the same d spacing of 2.46 Å assigned to the
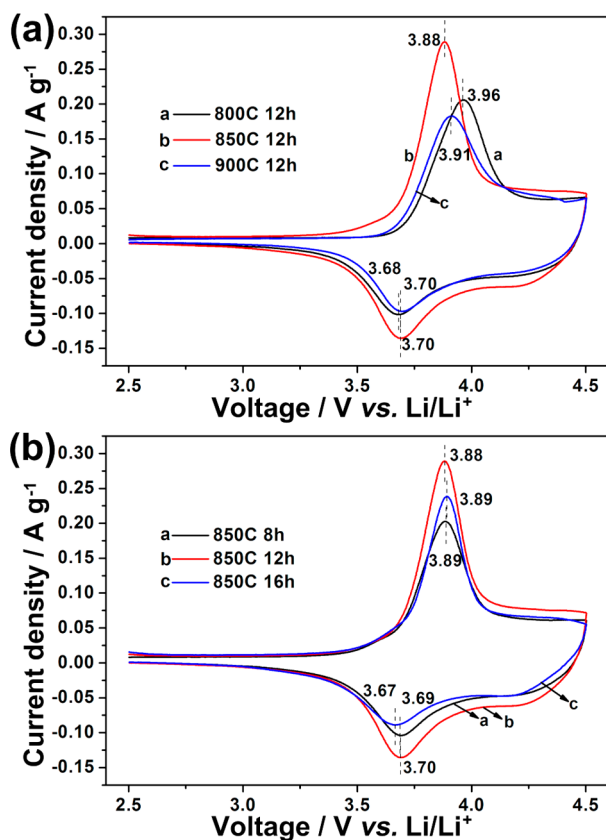
Figure 5. Cyclic voltammetry curves of all NCM nanoplates prepared at (a) different sintering temperatures and (b) different sintering times. The voltage range is 2.5−4.5 V, and the scan rate is 0.1 mV s^{-1}.

Figure 6. Nyquist plots of all NCM nanoplates prepared at (a) different sintering temperatures (b) different sintering times. The symbols are the experimental data, whereas the continuous lines are the fitted data.

(010) and (100) planes, respectively. And the other one has a *d* spacing of 1.43 Å assigned to (110) planes of NCM. The FFT pattern reveals these nanoplates are single crystalline with a hexagonal symmetry in consistence with the hexagonal structure of NCM. The HR-TEM image and the FFT pattern of the lateral plane (Figure 4d) show an interplanar distance of 4.75 and 2.44 Å assigned to the (003) and (101) planes of LiNi$_{1/3}$Co$_{1/3}$Mn$_{1/3}$O$_2$, respectively. This confirms the lateral plane is (0$\bar{1}$0) belonging to the {010} facets. This structural analysis indicates that the top and bottom planes of NCM-850-12H are {001} electrochemically inert planes and the lateral planes are electrochemically active {010} planes, which are perpendicular to the {001} planes. It suggests that there are more {010} planes exposed with the thickness of the NCM nanoplates increasing. Based on the analysis and the results of SEM, the new planes produced along the thickness direction in the NCM nanoplates calcined at 900 °C for 12h (NCM-900-12H) are non-{010} planes. Therefore, although the thickness of NCM-900-12H increases, the {010} planes decrease. NCM-850-16H has less {010} active facets than NCM-850-12H because its average thickness reduces. According to the above analysis, NCM-850-12H has the most {010} active planes, providing more channels for Li$^+$-ion transportation.

The initial cyclic voltammetry (CV) curves of all the as-prepared NCM nanoplates recorded in the voltage range of 2.5−4.5 V at the scan rate of 0.1 mV s^{-1} are shown in Figure 5. All the samples exhibit a pair of typical redox peaks for LiNi$_{1/3}$Co$_{1/3}$Mn$_{1/3}$O$_2$ system between 3.6 and 4.0 V.[10,12] The main difference of the CV profiles is the potential interval between the anodic and cathodic peaks which represents the
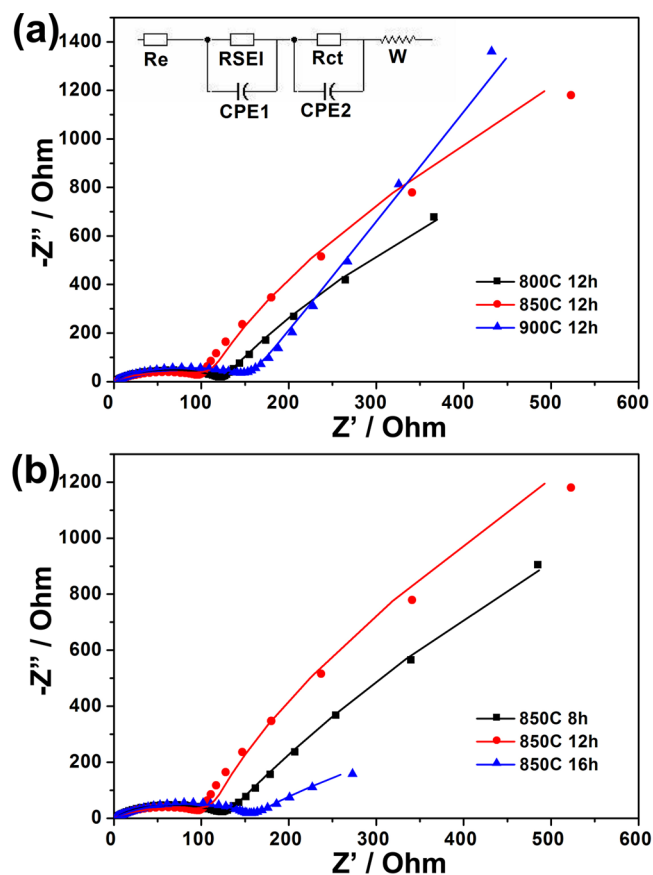
electrochemical process involving lithium diffusion in a solid phase and electron transfer across the electrode.[7] In all of the samples prepared at different sintering conditions, the NCM-850-12H displays the smallest potential interval (0.18 V), which indicates that the redox reaction and the transferring of electrons can be fast completed during the Li$^+$-ions intercalation/deintercalation process. In addition, the best defined and the symmetry of the CV peaks show the best reversibility during the charge/discharge process in the sample NCM-850-12H, which can be attributed to more {010} electrochemically active planes exposure.[9]

Electrochemical impedance spectroscopy (EIS) of all NCM nanoplates prepared at different sintering conditions was also investigated and the Nyquist plots are shown in Figure 6. The impedance parameters are fitted by the same equivalent circuit shown as the inset in Figure 6a. In all the Nyquist plots, there are three parts: a high-frequency intercept at the Z′ axis, a semicircle in the high-middle frequency region and a low-frequency oblique line. As it was described in the previous work,[10,22] the high-frequency intercept at the Z′ axis is the combined resistance of the electrolyte and cell components (R_e). The high-middle frequency semicircle is the contribution of two semicircles which are the solid electrolyte interface (SEI) resistance (RSEI) and the charge-transfer resistance (R_{ct}) in the electrode−electrolyte interfaces, respectively. The RSEI is corresponding to form a passive surface film on the surface of the cathode materials.[23] The low-frequency oblique line represents the Warburg impedance (*W*) due to the Li-ion
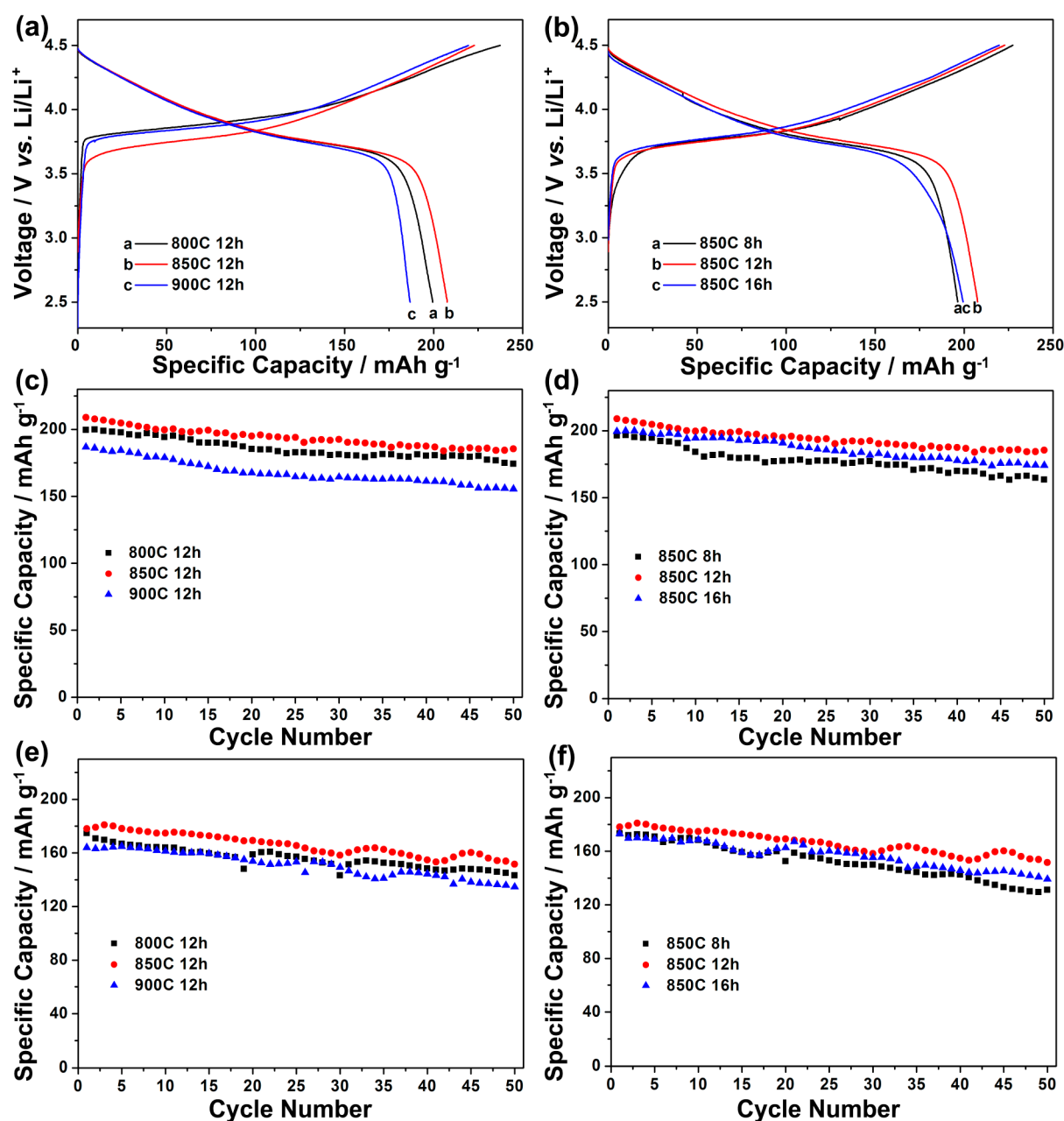
Figure 7. The electrochemical performances of all NCM nanoplates as cathodes for LIBs cycled in a voltage range of 2.5 and 4.5 V. (a, b) First galvanostatic charge/discharge curves at 0.1 C (20 mA g^{-1}). (c, d) Cyclability at 0.1 C. (e, f) Cycling performances at 1 C.

Table 2. Charge and Discharge Capacities, Coulombic Efficiencies and Capacity Retentions of NCM Nanoplates Cycled at 0.1 C

	1st cycle			50th cycle	
	charge capacity (mAh g^{-1})	discharge capacity (mAh g^{-1})	Coulombic efficiency (%)	discharge capacity (mAh g^{-1})	capacity retention (%)
NCM-800-12H	237.4	199.5	84.0	175.5	87.9
NCM-850-12H	222.9	207.6	93.1	185.5	89.4
NCM-900-12H	219.5	186.7	85.1	155.4	83.2
NCM-850- 8H	227.5	196.3	86.3	163.4	83.2
NCM-850-16H	219.8	199.4	90.7	174.1	87.3

diffusion process in the electrode materials. According to the EIS results, NCM-850-12H shows the lowest R_{ct} value (95.5 Ω) among all the NCM nanoplates, illustrating that the charge-transfer at the interface is faster than other NCM nanoplates. The lowest R_{ct} can be owing to that the more exposure of {010} electrochemically active planes can provide more

channels for Li$^+$-ion migration leading to faster charge-transfer reactions in the electrode−electrolyte interfaces for NCM-850-12H.

The electrochemical performances of all the NCM nanoplates were investigated using Li metal as anodes between 2.5 and 4.5 V. Figure 7a and b show the first charge/discharge

5080

dx.doi.org/10.1021/am500215b | ACS Appl. Mater. Interfaces 2014, 6, 5075−5082
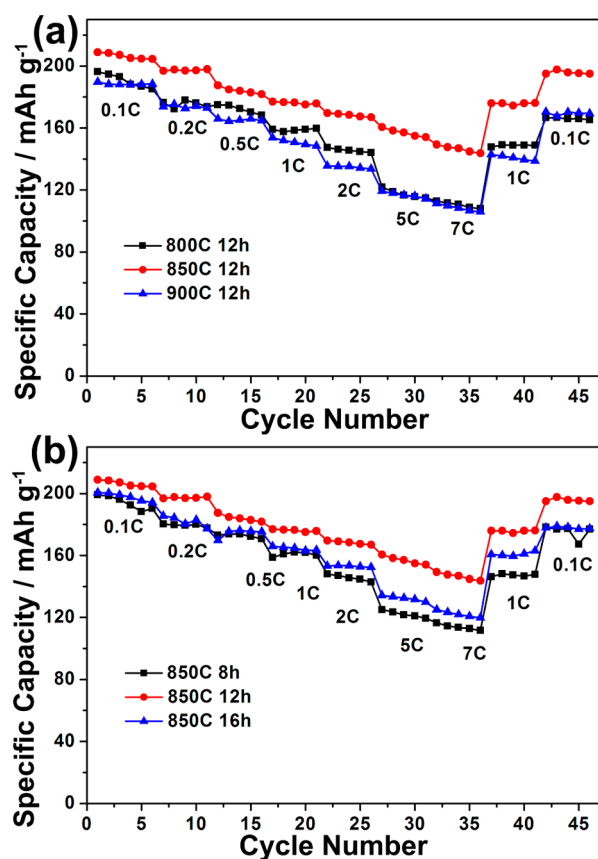
Figure 8. Rate capabilities of NCM nanoplates prepared at (a) different sintering temperatures and (b) different sintering times. The voltage range is 2.5−4.5 V and the current density is from 0.1 to 7 C.

curves of the NCM nanoplates cathodes at 0.1 C (1 C = 200 mA g^{-1}). It can be clearly observed that NCM-850-12H cathode shows a highest initial discharge capacity (207.6 mAh g^{-1}) and coulombic efficiency (93.1 %) among all the samples, higher than 197.9 mAh g^{-1} of NCM synthesized by traditional sol-gel method.[7] After 50 charge/discharge cycles at 0.1 C (Figure 7c, d), NCM-850-12H still maintains a discharge capacity of 180.3 mAh g^{-1} corresponding to a capacity retention of 89.4% which is the best among all the NCM nanoplates cathodes. The specific results are listed in Table 2. When the current density increases to 1 C (200 mA g^{-1}), the cycling performances of all NCM nanoplates are shown in Figure 7e, f. It is also evident that NCM-850-12H exhibits a higher discharge capacity (178.1 mAh g^{-1} at the initial cycle) and better cycle life (85.1% of capacity retention) than other NCM nanoplates cathodes.

Figure 8 displays the rate capabilities of all the NCM nanoplates cycled from 0.1 to 7 C between 2.5 and 4.5 V and the charge rates were equal to the discharge rates. When the charge−discharge rates were higher than 0.5 C, the voltage was kept at 4.5 V for 30 minutes after the constant current charge step to reach the predetermined voltage.[1] The results indicate that the discharge capacities of NCM-850-12H cathode are much higher than those of others at any current density attributing to the more exposure of {010} active facets. NCM-850-12H cathode shows discharge capacities of 169.8, 160.5, and 149.3 mAh g^{-1} at 2, 5, and 7 C, respectively, which are higher than those of NCM nanobricks with the {010} active facets prepared through PVP-assisted co-precipitation process.

This is because the NCM nanoplates have large amounts of pores between the nanoplates and the NCM nanobricks are aggregated with each other.[9] The porous structure enables the electrolyte penetration facile through the voids between the nanoplates. When the current rate is reduced back to 1 and 0.1 C, the capacities can return to almost the initial values, suggesting good reversibility for NCM nanoplates.

Compared to other NCM cathodes,[7−12] NCM-850-12H cathode also delivers the superior electrochemical performance, which can be attributed to the special single-crystalline nanoplate structure with more {010} active facets exposed. First, the small size and the porous structure of NCM nanoplates enable facile electrolyte penetration through the voids between the nanoplates and short distances for Li$^+$-ion transportation. Second, the exposure of the {010} active facets can provide more channels for Li$^+$-ion discussion. Third, the high-quality crystallinity of the nanoplates guarantees the stability of the crystallographic structure for NCM during cycling.[24]

To verify the structural stability of the NCM nanoplates, we opened the cells and measured the morphologies of all samples after electrochemical cycling. The SEM images of all NCM nanoplates after 50 charge/discharge cycles at 1 C between 2.5 and 4.5 V are shown in Figure S3 in the Supporting Information. The results suggest that all the NCM nanoplates can maintain their initial nanoplates morphologies through the charge/discharge processes. Hence, the NCM nanoplates are very stable.

◼ CONCLUSION

Hexagonal layered NCM nanoplates exposed {010} active facets are successfully synthesized in ethylene glycol medium. From the SEM and HR-TEM results, the amounts of {010} facets is raised with the thickness of NCM nanoplates increasing. However, when calcined at 900 °C, some of layered structures start transforming into spinel ones leading to many non-{010} crystal planes along the thickness direction, which makes the {010} facets decrease. Among the NCM nanoplates prepared under various sintering conditions, NCM-850-12H exhibits the best electrochemical performance as a cathode for LIBs owing to the most exposure of {010} planes. It shows a high first discharge capacity (207.6 mAh g^{-1} at 0.1 C) and an excellent rate capability (169.8, 160.5, and 149.3 mAh g^{-1} at 2, 5, and 7 C, respectively), which are higher than most of NCM cathodes.

◼ ASSOCIATED CONTENT

ⓢ Supporting Information

Thickness distribution, average thickness of all the NCM nanoplates, and SEM images after 50 charge/discharge cycles at 1 C. This material is available free of charge via the Internet at http://pubs.acs.org.

◼ AUTHOR INFORMATION

Corresponding Author
*E-mail: cbcao@bit.edu.cn.

Notes
The authors declare no competing financial interest.

■ REFERENCES

(1) Zhou, L.; Zhao, D.Y.; Lou, X. W. $LiNi_{0.5}Mn_{1.5}O_4$ Hollow Structures as High-Performance Cathodes for Lithium-Ion Batteries. *Angew. Chem.* **2012**, *124*, 243−245; *Angew. Chem., Int. Ed.* **2012**, *51*, 239−241.

(2) Armand, M.; Tarascon, J. M. Building Better Batteries. *Nature* **2008**, *451*, 652−657.

(3) Arić, A. S.; Bruce, P.; Scrosati, B.; Tarascon, J. M.; Van Schalkwijk, W. Nanostructureed Materials for Advanced Energy Conversion and Storage Devices. *Nat. Mater.* **2005**, *4*, 366−377.

(4) Tarascon, J. M.; Armand, M. Issues and Challenges Facing Rechargeable Lithium Batteries. *Nature* **2001**, *414*, 359−367.

(5) Zhu, J. X.; Vo, T.; Li, D. S.; Lu, R.; Kinsinger, N.; Xiong, L.; Yan, Y.S.; Kisailus, D. Crystal Growth of $Li[Ni_{1/3}Co_{1/3}Mn_{1/3}]O_2$ as a Cathode Material for High-Performance Lithium Ion Batteries. *Cryst. Growth Des.* **2012**, *12*, 1118−1123.

(6) Lee, S.; Park, S. S. Atomistic Simulation Study of Mixed-Metal Oxide ($LiNi_{1/3}Co_{1/3}Mn_{1/3}O_2$) Cathode Material for Lithium Ion Battery. *J. Phys. Chem. C* **2012**, *116*, 6484−6489.

(7) Gao, P.; Li, Y. H.; Liu, H. D.; Pinto, J.; Jiang, X. F.; Yanga, G. Improved High Rate Capacity and Lithium Diffusion Ability of $LiNi_{1/3}Co_{1/3}Mn_{1/3}O_2$ with Ordered Crystal Structure. *J. Electrochem. Soc.* **2012**, *159*, A506−A513.

(8) Ding, Y.; Zhang, P.; Long, Z.; Jiang, Y.; Gao, D. The Morphology, Structure and Electrochemical Properties of $LiNi_{1/3}Co_{1/3}Mn_{1/3}O_2$ Prepared by Electrospun Method. *J. Alloys Compd.* **2008**, *462*, 340−342.

(9) Fu, F.; Xu, G.-L.; Wang, Q.; Deng, Y.-P.; Li, X.; Li, J.-T.; Huang, L.; Sun, S.-G. Synthesis of Single Crystalline Hexagonal Nanobricks of $LiNi_{1/3}Co_{1/3}Mn_{1/3}O_2$ with High Percentage of Exposed {010} Active Facets as High Rate Performance Cathode Material for Lithium-Ion Battery. *J. Mater. Chem. A* **2013**, *1*, 3860−3864.

(10) Li, J.L.; Cao, C.B.; Xu, X.Y.; Zhu, Y.Q.; Yao, R.M. $LiNi_{1/3}Co_{1/3}Mn_{1/3}O_2$ Hollow Nano-micro Hierarchical Microspheres with Enhanced Performances as Cathodes for Lithium-Ion Batteries. *J. Mater. Chem. A* **2013**, *1*, 11848−11852.

(11) Yang, C.F.; Huang, J.J.; Huang, L.G.; Wang, G.J. Electrochemical Performance of $LiCo_{1/3}Mn_{1/3}Ni_{1/3}O_2$ Hollow Spheres as Cathode Material for Lithium Ion Batteries. *J. Power Sources* **2013**, *226*, 219−222.

(12) Huang, Z.-D.; Liu, X.-M.; Oh, S.-W.; Zhang, B.; Ma, P.-C.; Kim, J.-K. Microscopically Porous, Interconnected Single Crystal $LiNi_{1/3}Co_{1/3}Mn_{1/3}O_2$ Cathode Material for Lithium Ion Batteries. *J. Mater. Chem.* **2011**, *21*, 10777−10784.

(13) Shaju, K. M.; Bruce, P. G. Macroporous $Li(Ni_{1/3}Co_{1/3}Mn_{1/3})O_2$: A High-Power and High-Energy Cathode for Rechargeable Lithium Batteries. *Adv. Mater.* **2006**, *18*, 2330−2334.

(14) Wei, G.-Z.; Lu, X.; Ke, F.-S.; Huang, L.; Li, J.-T.; Wang, Z.-X.; Zhou, Z.-Y.; Sun, S.-G. Crystal Habit-Tuned Nanoplate Material of $Li[Li_{1/3-2x/3}Ni_xMn_{2/3-x/3}]O_2$ for High-Rate Performance Lithium-Ion Batteries. *Adv. Mater.* **2010**, *22*, 4364−4367.

(15) Azib, T.; Ammar, S.; Nowak, S.; Lau-Truing, S.; Groult, H.; Zaghib, K.; Mauger, A.; Julien, C.M. Crystallinity of Nano C-$LiFePO_4$ Prepared by the Polyol Process. *J. Power Sources* **2012**, *217*, 220−228.

(16) Lim, J.; Gim, J.; Kang, J.; Song, J.; Park, H.; Baek, S.; Kim, J. Synthesis of $LiFePO_4$ Using Fe^{3+} Precursors in Polyol Medium. *J. Electrochem. Soc.* **2012**, *159*, A459−A463.

(17) Pieczonka, N. P. W.; Liu, Z.; Huq, A.; Kim, J.-H. Comparative Study of $LiMnPO_4$/C Cathodes Synthesized by Polyol and Solid-State Reaction Methods for Li-Ion Batteries. *J. Power Sources* **2013**, *230*, 122−129.

(18) Jin, R. C.; Liu, Z. Q.; Yang, L. X.; Liu, J. S.; Xu, Y. B.; Li, G. H. Facile Synthesis of Sulfur Doped Sb_2Se_3 Nanosheets with Enhanced Electrochemical Performance. *J. Alloys Compd.* **2013**, *579*, 209−217.

(19) Bréger, J.; Dupré, N.; Chupas, P. J.; Lee, P. L.; Proffen, T.; Parise, J. B.; Grey, C. P. Short- and Long-Range Order in the Positive Electrode Material, $Li(NiMn)_{0.5}O_2$: A Joint X-ray and Neutron Diffraction, Pair Distribution Function Analysis and NMR Study. *J. Am. Chem. Soc.* **2005**, *127*, 7529−7537.

(20) Rao, C. V.; Reddy, A. L. M.; Ishikawa, Y.; Ajayan, P. M. $LiNi_{1/3}Co_{1/3}Mn_{1/3}O_2$-Graphene Composite as a Promising Cathode for Lithium-Ion Batteries. *ACS Appl. Mater. Interfaces* **2011**, *3*, 2966−2972.

(21) Li, N.; Mei, T.; Zhu, Y.C.; Wang, L.L.; Liang, J.W.; Zhang, X.; Qian, Y.T.; Tang, K.B. Hydrothermal Synthesis of Layered $Li_{1.81}H_{0.19}Ti_2O_5 \cdot xH_2O$ Nanosheets and Their Transformation to Single-Crystalline $Li_4Ti_5O_{12}$ Nanosheets as the Anode Materials for Li-Ion Batteries. *CrystEngComm* **2012**, *14*, 6435−6440.

(22) Shaju, K. M.; Subba Rao, G. V.; Chowdari, B. V. R. Influence of Li-Ion Kinetics in the Cathodic Performance of Layer Li-$(Ni_{1/3}Co_{1/3}Mn_{1/3})O_2$. *J. Electrochem. Soc.* **2004**, *151*, A1324−A1332.

(23) Bie, X.F.; Du, F.; Wang, Y.H.; Zhu, K.; Ehrenberg, H.; Nikolowski, K.; Wang, C.Z.; Chen, G.; Wei, Y.J. Relationships Between the Crystal/Interfacial Properties and Electrochemical Performance of $LiNi_{0.33}Co_{0.33}Mn_{0.33}O_2$ in the Voltage Window of 2.5−4.6 V. *Electrochim. Acta* **2013**, *97*, 357−363.

(24) Ding, Y. L.; Xie, J.; Cao, G. S.; Zhu, T. J.; Yu, H. M.; Zhao, X. B. Single-Crystalline $LiMn_2O_4$ Nanotubes Synthesized Via Template-Engaged Reaction as Cathodes for High-Power Lithium Ion Batteries. *Adv. Funct. Mater.* **2011**, *21*, 348−355.